Reeves, et al., J. Geophys. Res., 97, 6219, 1992.

The Great Solar Energetic Particle Events of 1989 Observed From Geosynchronous Orbit

G. D. REEVES, T. E. CAYTON, S. P. GARY, AND R. D. BELIAN

Los Alamos National Laboratory, Los Alamos, New Mexico

Los Alamos energetic proton instruments at geosynchronous orbit observed more major solar energetic particle events during 1989 than any other year since this series of detectors began observations in 1976. The temporal flux profiles of four intervals, which contain six distinct events, are compared illustrating the uniqueness of each event. Characteristic risetime and decay time are computed for each event. During two of these events, brief order-of-magnitude increases of the proton flux are observed. They are associated with sudden commencement events and dramatic changes in the solar wind. We conclude that these two brief events are likely the result of shock acceleration in the solar wind. We have fit the measured count rates to a spectral form which is exponential in rigidity, and we have examined the changes in spectral slope with time for each of the four intervals. In general, harder spectra are measured near the onset of an event followed by a softening of the spectrum as the fluxes decay. We have also investigated the effects of these events on geomagnetic activity by comparing the fluxes of >30-keV electrons at geosynchronous orbit and *Kp* geomagnetic index during the early part of two of the solar energetic particle events.

INTRODUCTION

Solar cycle 22, which started with the sunspot minimum in October 1986, has thus far posed an unprecedented threat to space communications, orbital assets, and Earth-based electrical systems [*Gorney,* 1990]. The year 1989 saw an exceptionally large number of sunspots and solar flares, energetic particle events in the near-Earth space environment, and ground level neutron enhancements [*Bieber et al.*, 1990]. These phenomena are of course related; solar flares generate large numbers of energetic particles, some of which escape into interplanetary space. A solar energetic particle (SEP) event observed by spacecraft in interplanetary space or in the near-Earth space environment will have properties determined not only by the flare source mechanism but also by the properties of the interplanetary medium. Scatter-free events propagate in a relatively direct manner from the Sun and to some extent reflect accelerated particle characteristics at the solar source. Particles corresponding to diffusive events have suffered relatively substantial scattering by magnetic fluctuations in the interplanetary environment [*Beeck et al.,* 1990, and references therein].

Not all SEP events are observed at Earth. An SEP event is termed well connected if the Earth lies directly in the path of the energetic particles. For poorly connected events, only peripheral contact may occur. The nominal path of propagation is along the Archimedean spiral of the solar wind although this path may be perturbed by magnetic turbulence, variable solar wind speed or density, or scattering and diffusion. The effects observed on a spacecraft or at Earth depend not only on the general propagation of the particles but also on the degree of connectivity between the source and the observation point. The degree of contact and the amount of scattering between the source and the Earth contribute to the temporal characteristics of the observations and the effects produced at the Earth.

Entry to and transport within the Earth's magnetosphere also affects energetic particles. The main effects are expected to be an isotropization of the fluxes and filtering out of some of the high-frequency features which might have been present in the solar wind. Both effects as well as the depth of penetration into the magnetosphere are energy dependent. (See *Morfill and Scholer* [1973] for an extensive review.) Thus, while fluxes of greater than 10-MeV protons at geosynchronous orbit closely resemble fluxes in the solar wind, they are not identical.

Studies of solar energetic particle events have a long history and a rich bibliography. Even an adequate review would be too lengthy for this brief report. We direct the reader to two excellent reviews of SEP events: *McCracken and Rao* [1970] and the more contemporary review of *Smart and Shea* [1989].

This paper describes the most significant of the energetic particle events of 1989, as observed by Los Alamos energetic particle instruments at geosynchronous orbit. Each of the events differs in important respects from the others. We draw attention to the temporal characteristics of the events which characterize the degree of connectivity to the source and the amount of scattering which occurred. We also compare the effects of two events on the Earth's magnetosphere as measured by geomagnetic activity. Brief order-of-magnitude increases in energetic proton flux are found in two of the events, and we discuss their relationship to the passage of interplanetary shocks.

Using a computer model of the instrument response up to several GeV and the measured count rates, we are able to determine best fit spectra assuming the spectra have the form of an exponential in rigidity. This allows us to compare the hardness of the energetic proton spectra for each event as a function of time. Again, the uniqueness of each event, the dependence on source and propagation characteristics, and the dramatic temporal evolution are apparent.

INSTRUMENTS

Since 1976 Los Alamos National Laboratory has flown the charged particle analyzer (CPA) sensor systems for the measurement of energetic charged particles at geostationary orbit. Energetic protons are measured in the spacecraft equatorial plane by the high-energy proton (HiP) instrument subsystem. It has an active guard scintillator and a sweeping magnet to eliminate contamination from electrons below about 1 MeV. The HiP uses three detectors in a telescope configuration to record protons in 16 differential energy channels. Although the thresholds vary slightly from spacecraft to spacecraft, for this study we used data from the instrument on spacecraft 1987-097 for which the nominal energy thresholds were 0.37, 0.48, 0.67, 0.85, 1.03, 1.33, 1.72, 2.60, 4.74, 8.96, 13.6, 23.9, 36.4, 58.3, 83.8, and 147 MeV; 160 MeV is the upper energy cutoff. Electrons with energies from 30 to 300 keV are measured by the LoE subsystem in six nested integral energy bands. This instrument utilizes five telescopes which have look angles of 0°, ±30°, and ±60° with respect to the spacecraft equatorial plane. The spacecraft spin axis points toward the Earth so nearly complete pitch angle coverage is obtained in each 10-s spin. Each energy band is sampled for 8 ms, but data are typically presented at 10-s, 1-min, and 1-hour averages. Two other instrument subsystems which measure higher-energy electrons and lower-energy protons are not used in this analysis. A more complete description of the CPA instruments may be found in the paper by *Baker et al.* [1979].

Previous energetic proton studies based on data from the CPA detectors include *Belian et al.* [1978, 1984], *Baker et al.* [1979], and *Reeves et al.* [1990*a*, 1990*b*]. Except for Baker et al., these studies have considered only protons below 1 MeV; the present work is the first to examine CPA data at energies well above that number. A complimentary study by R. D. Belian et al. (High *Z* energetic particles at geosynchronous orbit during the great solar proton event of October 1989, submitted to *Journal of Geophysical Research*, 1992) utilizes a new generation of instruments to examine the composition of solar energetic ions observed at geosynchronous orbit in October 1989.

TEMPORAL STRUCTURE

Figure 1 shows one hour averaged fluxes of protons with energies greater than 10 MeV from the CPA instrument on spacecraft 1987-097 for the year 1989. These fluxes are calculated by summing HiP channels from 10 to approximately 160 MeV. Fluxes of protons with energies above 160 MeV do not contribute appreciably to the sum.

During six intervals in 1989, proton fluxes in this energy range surpassed 10^3 (cm^2 s sr)$^{-1}$, and during one interval fluxes approached 10^5 (cm^2 s sr)$^{-1}$. Within each interval there may be several distinct events, each producing a peak in the flux profile measured at geosynchronous orbit. The source of the energetic particle events is typically a solar flare although other sources have occasionally been identified [*Kahler et al.*, 1986].

In this paper we have selected four of the most significant 10-day intervals for comparison. The intervals of interest begin on March 6 (day 65), August 12 (day 224), September 27 (day 270), and October 18 (day 291) and are shown in 1-hour resolution in Figure 2. The data are all from spacecraft 1987-097. Across the top of each plot, there are triangles indicating the onset of Hα flare activity during the selected intervals (Solar Geophysical Data Prompt Reports, 1989). The source flares for peak fluxes which exceed 10^3 (cm^2 s sr)$^{-1}$ are indicated by solid black triangles while other flares are identified by shaded gray triangles. The flares we indicate here as source flares are those identified in Solar Geophysical Data Prompt Reports (Table of Solar Proton Events Affecting the Earth Environment, p. 151.) Clearly, each of the other flares during these intervals is also a potential source of energetic protons.

Also shown by plus symbols on Figure 2 are the time and intensity of proton flux maxima derived from the GOES spacecraft data (Solar Geophysical Data Prompt Reports, 1989). Differences in flux magnitude are the result of differences in spacecraft location and instrument calibration and are the subject of ongoing scrutiny.

An SEP event usually exhibits a rapid rise and a slower decline of energetic proton fluxes. Table 1 gives the time and intensity of maximum, the fluence above 10 MeV, the characteristic risetime and decay time, and location of the source flare for each of the six events illustrated in Figure 2. The time of maximum (T_{max}) and maximum fluxes are based on 1-hour averages of the CPA data. The fluence is the integral of the 1-hour average fluxes. For purposes of comparison we consider only the 10-day intervals plotted in Figure 2. The value 2.17×10^9 (cm^2 sr)$^{-1}$ is the integral over the October A, B and C events. We also note that at the end of these 10-day intervals the energetic proton fluxes have not returned to their background levels so the fluence values somewhat underestimate the total fluence. In fact, for the October event, another small enhancement was observed on October 29 which lies outside the interval we consider.

Risetimes

The characteristic risetime and decay time in Table 1 are *e*-folding times and were calculated from 1-min averaged CPA data. Each event, except March, exhibits a rapid exponential rise early in the event. Since these measurements were taken within the Earth's magnetosphere, they are expected to be similar to, but perhaps slightly longer than, risetimes in the solar wind. A several hour period during which the exponential slope was the most constant was used to determine the risetimes.

The risetime is primarily a function of the proton spectrum, the distance traveled, and amount of coronal diffusion. Coronal diffusion is a function of the angle, Φ, between the flare and the solar foot point of the interplanetary magnetic field line connected to the Earth. (Nominally, the field line is an Archimedian spiral with the foot point of the field for a 404 km/s solar wind speed at

solar longitude, ϕ=57.2°W [*Smart and Shea,* 1985].) Thus events with large ϕ are expected to suffer from large coronal diffusion and to be observed with longer risetimes. From Table 1 we see that these six events do not follow the expected dependance of risetime on source flare longitude. For example, the flux peak of the October B event has a faster risetime than the other two peaks in October suggesting that the foot point of the interplanetary magnetic field (IMF) line is further east than the nominal 57.2°W location.

The risetime of the flux in the September event was also exceptionally fast. Within a span of only a few hours fluxes of >10-MeV protons jumped from the order of 1 $(cm^2\ s\ sr)^{-1}$ to over 10^4 $(cm^2\ s\ sr)^{-1}$. It is notable, however, that the source was observed on the western limb and probably originated in an active region which had rotated out of view. This suggests that for this event the foot point of the IMF was significantly west of its nominal position.

Such discrepancies with the nominal behavior of solar energetic particle events is not unusual. Deviations from nominal behavior are principally due to the fact that the solar wind is often significantly disturbed by dramatic solar activity. Disturbances within the solar wind typically follow the arrival of the first energetic particles due to the lower energy of the bulk plasma. Therefore such effects are more clearly seen in the later events in a series. For example, the October A event was preceded by a flare which contributed no noticeable energetic protons at Earth. It did, however, increase the solar wind velocity from approximately 400 km/s prior to the October A onset to nearly 600 km/s at the time of onset which could affect the observed risetime. (Solar wind data are from the IMP 8 Faraday cup (Solar Geophysical Data Prompt Reports, 1989) and electrostatic analyzer (J. A. Gosling, personal communication, 1991).)

Although there is no solar wind data for day 224 (August 12), we suspect that propagation effects play a role in the length of the risetime. Figure 3 shows the rising portions of the August and October events in 1-min time resolution. In August the fluxes rise, dip again between 2200 and 2400 UT and then rise again. Our calculation of the risetime is clearly affected by this behavior which is likely to be the result variable solar wind conditions.

The risetime calculated for the March interval must be interpreted differently than for the other events. Solar wind data are not available for most of this period, but we suspect that the narrow peak in the flux profile is caused by acceleration of particles in the solar wind rather than at the Sun. The observation of magnetospheric sudden commencements preceding and following the energetic proton peak suggest that it may have been produced by converging shocks in the solar wind. Nine *X* class flares were observed during these 10 days (as shown in Figure 2). All were produced by the same solar active region which rotated from 69° E to 21° W from the first to the last flares shown. Thus the risetime calculated for the March event probably includes the effects of changing connectivity and a variable solar wind (as seen in data for the first few days of the interval) as well as multiple sources.

Decay Times

The decaying portion of an SEP event is typically approximately exponential as is illustrated by the October B and C events in Figure 2. The decay time was calculated from the average exponential slope over approximately 1-day intervals following the peaks. The characteristic decay time can be modeled based on the diffusion of particles in the interplanetary medium and is found to depend on the distance traveled, the solar wind velocity, and the differential energy spectral component (which is also a function of ϕ) [*Roelof and Krimigis,* 1973]. Flares in the eastern solar hemisphere rotate toward the foot point and ideally should have a slower decay rate. However, the events studied here do not follow that statistical trend. Again, deviation from the classic flux profiles is generally caused by propagation effects in the solar wind [*McCracken et al.*, 1970]. For example, the initial decay of the September event was fairly rapid but then changed abruptly at day 275 when a much slower decay followed. This signature is most often associated with the effects of a coronal mass ejection (CME) which is ahead of the Earth in its orbit [*Cane et al.*, 1988]. Early in the event energetic particles have relatively direct access to the Earth. As the CME moves out away from the Sun, field line draping produces poorer magnetic connection.

For the August event the fluxes show considerable variation from an exponential decay. The fluxes initially decay after the peak on day 225 (August 13) but then rise again on day 226. The later peak precedes the flare early on that day so it is clearly not an injection of new flare particles. Rather, we find that this feature is associated with an increase in the solar wind speed from ≈400 km/s to ≈600 km/s.

The March event is as unusual in its decay phase as it is in its rising phase. Fluxes dropped 3 orders of magnitude in less than one day following the peak on day 72 (March 13). This is primarily a result of the sharpness of that peak which accentuates the slope of the decay phase. It is notable that without the presence of this peak energetic proton fluxes would not even have surpassed 10^3 $(cm^2\ s\ sr)^{-1}$.

The flux profile in October shows a similar, brief, order-of-magnitude flux increase late in day 293. Our analysis of the onset of the abrupt flux increase for different energy bands (data not shown) reveals no energy dispersion. This suggests that the process which produced this feature took place locally, near the Earth, rather than near the Sun. IMP 8 data shows an increase in solar wind velocity from less than 500 km/s to over 800 km/s on this day. Thus the increase could be caused by a compression of the solar wind.

Another interpretation is that it is caused by shock acceleration in the solar wind [e.g., *Cane et al.*, 1988]. Figure 3 shows this flux increase following onset in 1-min resolution. At approximately 1200 UT the >10-MeV proton fluxes began to increase to a level an order of magnitude over previous levels. The most rapid variation

occurred at approximately 1400 UT when flux levels jumped almost a factor of 5 in a span of several minutes. This flux increase was preceded by a sudden commencement event observed at Earth at 0916 UT in association with the passage of an interplanetary shock (upward pointing arrow in Figure 3). The time delay of approximately 3 hours between the sudden commencement and the increase in >10-MeV proton flux is unexplained at present but may be related to the changing magnetic connection between the Earth and the shock acceleration region. It appears that while the flare on day 291 produced no discernable flux of energetic protons at Earth, it was this flare which was responsible for the shock which arrived on day 293 and thus still had a rather dramatic effect on the magnitude of this SEP event. Such order-of-magnitude increases are quite important because the elevated fluxes can suddenly reach even higher levels which are a threat to systems on the ground or instruments and humans in space. Furthermore, without a monitor upstream of the Earth, their arrival is unpredictable.

Geomagnetic Activity

Figure 3 compares the flux profiles of the early parts of the August and October A events in 1-min resolution. The upper curve shows fluxes of greater than 30-keV electrons, and the lower curve shows greater than 10-MeV protons. In the lower panel in each plot, 3-hour *Kp* indices are plotted over a 2-day interval. This figure compares not only the very energetic proton fluxes observed in these two events but also the geomagnetic effects of the events.

The exponential rise and leveling off of the proton flux is seen clearly for both events. In the early stages of each event the trapped >30-keV electron population exhibits typical flux levels around 10^7 cm^2 s sr)$^{-1}$ with small variations produced by moderate levels of geomagnetic activity. Magnetic *Kp* levels for both events were moderate around the onset of energetic proton enhancements reflecting the fact that protons of these energies do not produce geomagnetic activity. Significant geomagnetic activity is more likely to be produced by less energetic, more dense plasma, the arrival of which is delayed with respect to the onset of energetic particle fluxes. One effect can be seen at the time of the sudden commencement on day 293 (Figure 3) when the flux of >30-keV trapped electrons dropped precipitously as the magnetosphere was compressed and the spacecraft found itself at higher *L* shells. Very high levels of *Kp* were observed following the passage of the shock. The high level of geomagnetic activity is also evident in the >30-keV electron fluxes which show a series of intense modulations produced by substorms.

In August, by contrast, only moderate fluctuations in the >30-keV electron fluxes are observed after the energetic proton flux onset. This event was not geomagnetically effective – a fact reinforced by the presence of moderate to low *Kp* values (Figure 3).

A similar pattern was exhibited by the high-resolution data for March and September (not shown). From the available data the solar wind appears to have been fairly steady and of moderate velocity throughout the September event and geomagnetic activity remained at levels below *Kp*=3. In March, on the other hand, the solar wind was very disturbed producing dramatic geomagnetic activity with *Kp*=9 and strong modulations in the trapped electron flux as well as producing large perturbations of the solar energetic proton fluxes.

Spectral Slope

The HiP instrument has six energy channels which are sensitive to protons with energies above 10 MeV. The data from these six channels can be used to obtain the spectra of solar energetic protons arriving at geosynchronous orbit. In a first-order analysis, one could assign each channel an energy, convert counts to flux based on the nominal geometric factor of the telescope, graph the points, and call that the spectrum. However, this would ignore several instrumental realities. Shielding for protons with energies greater and perhaps much greater than 10 MeV is not totally effective. Therefore the geometric factor is a somewhat complex function of energy. As a corollary, each channel can count protons outside its nominal energy range. Assigning an average energy to each channel requires a knowledge of both its response as a function of energy and the shape of the spectrum.

What we have done to avoid this circular dependence is to assume a spectral form and derive a best fit to that form using the measured count rates. The spectral form we have chosen is an exponential in proton rigidity, $F \propto \exp(\gamma R)$, where $R = pc/q$ is the rigidity or relativistic momentum per charge [e.g., *Freier and Webber,* 1963, *McGuire and von Rosenvinge*, 1984]. This form of the spectrum is also commonly expressed as $F \propto \exp(-R/R_0)$.

The response functions were obtained by running a three dimensional, Monte Carlo transport code called TRIM [*Ziegler et al.,* 1985]. The TRIM code uses the full instrument and detector geometry and calculates the response to protons of up to several GeV (including side penetraters) for each channel. In our application we assumed an isotropic particle source.

Using the measured count rates and knowing the instrument response over the full energy range allows us to find a best fit spectral slope. An assumed spectrum (for a given slope, γ) convolved with the instrument response gives a simulated count rate for each channel which can be compared with the measured count rate. The γ which minimizes the difference between the measured and model count rates is the best fit spectral slope for the spectral form assumed. Figure 4 shows the result of this analysis. Plotted are the average measured and model count rates for 1 hour of data centered on day 293, 1507 UT which is the peak of the shock-related flux increase in the October A event. The slope which gives this fit is γ = -10.45 GV^{-1} (R_0 = 95.7 MV). The difference between the measured HiP counts and model "best fit" counts is a

measure of the accuracy of the determination of the slope and the assumed spectral form.

It is also possible to deconvolve the count rates and the instrument response to obtain a spectrum. The technique we use here assumes that we know what percentage of the counts in a given channel came from each energy that contributed to the total count rate. We assume that counts are apportioned to the measured count rate in the same proportions as the model counts which were obtained from the best fit exponential spectrum. This method is not very general but will reveal gross deviations if the true spectrum were not exponential. Two spectra are plotted in Figure 5. Fluxes are plotted at each rigidity for which the instrument response was calculated. The straight lines are the model spectra in the form $F = J_o \exp(\gamma R)$ with the γ and J_o which give the best fit to the measured counts. The unconnected symbols give the synthetic spectrum derived by apportioning the measured counts to each rigidity. Although this method inclines the data to fall along the exponential fit it does not require that they do so and small, systematic deviations from an exponential form are apparent over certain rigidity ranges.

The solid circle symbols are for a 1-hour average on day 292, 1800 UT which was near the onset of the October A event. It reveals a hard spectrum with γ = -5.27 GV^{-1} (R_0 = 190 MV). The plus symbols are for day 293, 1507 UT which is the same interval as shown in Figure 4 – the peak of the shock-related flux increase. We can see that, although total fluxes are higher during that period than near the onset of the October A event, the spectrum is considerably softer.

This and other spectral characteristics are illustrated in Figure 6 which shows the best fit spectral slope for each hour average of data throughout each interval (upper panels) and the >10-MeV fluxes (lower panels). The clearest signature of the arrival of solar protons is seen in the October interval. Here the very low flux levels observed before the arrival of the solar protons are seen to have a fairly hard spectrum, $\gamma = -7$ ($R_0 = 143$ MV). The onset of arrival of protons from each solar energetic particle event is accompanied by increasing hardness of the spectrum. A more detailed examination of the timing (not shown) reveals that the spectral slope increases before the fluxes increase and that by the time the peak fluxes are observed the spectral slope has decreased dramatically. This is to be expected. The most energetic particles arrive first and produce a dramatic hardening of the spectrum but not much change in flux since their numbers are small. The arrival of the more plentiful, lower energy particles softens the spectrum but dramatically increases the flux.

It is also apparent from this figure that the shock-related flux increase on day 293 (October 20) is not accompanied by a hardening of the spectrum. The spectral slope continues to decline steadily, or may even dip slightly. The lack of hardening is further evidence that the flux increase is not due to new solar particles but rather to ion acceleration in the solar wind. A new burst of solar particles is expected to harden the spectrum as seen at the onset of the events we have identified. On the other hand, a clearer softening of the spectrum is expected from shock acceleration than was observed at this time. A clear example is seen on day 67 (March 8) when the passage of an interplanetary shock produced a dramatic softening of the spectrum (but in this case not much change in the energetic proton fluxes.) It is possible that the lack of softening of the spectrum is a result of our technique to determine the spectral slope and our assumption of an exponential form. Figure 4 (which shows data taken during the October flux increase) suggests that the best fit counts may overestimate the hardness of the spectrum when the count rates are not monotonically decreasing with energy.

The intensity of the highest end of the proton spectrum can be measured from the ground. The upward pointing triangles in Figure 6 mark the times of ground level enhancements (GLEs) seen in neutron flux monitors at Calgary [*Mathews and Venkatesan,* 1990]. Those times are also in Table 2. The intensity for GLEs is given as a percentage increase above the average counting rate before the event. Notice that the three GLEs observed in October correspond very well with the three main flux onsets and increases in spectral hardness.

The September event produced fluxes which have a hardness even greater than the October events. However, because the preevent fluxes, which are cosmic ray background, were equally hard, the onset is not as apparent. Onset in the September event was also accompanied by a GLE which increased neutron fluxes at Calgary by over 400%. GLEs are only produced by protons with energies greater than 0.5 GeV which then produce a cascade of secondary particles as they interact in the upper atmosphere. Therefore the large increase in neutron fluxes in September corresponds with the exceptional hardness of the spectrum. In fact, a GLE was also observed for this event in New Mexico where the lower magnetic latitude requires incident particles of greater than 20 GeV [*Mathews and Venkatesan,* 1990]. We also note that the change in the decay rate of the September fluxes, which we earlier associated with the passage of a CME, coincides with a hardening of the spectrum but no injection of new particles.

The August event is, overall, considerably softer – both before the event and at its onset. A distinct hardening of the spectrum is observed in association with a subsequent flare early in day 228 (August 16). A comparison with Figure 2 shows that this is the only flare in the interval which produces a GLE which again is consistent with a significant high-energy component in the spectrum. While rapid variations in the spectral slope early in each of these intervals is due to very low count rates (and therefore statistical noise) the rapid variations in the spectral slope prior to August 16 occur during periods of high flux and are the result of continuing solar wind disturbance.

The large and dynamic variation in the spectral slope for the March event emphasizes the complexity inherent in events with multiple sources which propagate through a disturbed medium. Softer spectra are observed at the times of maximum flux again suggesting shock-related effects. Ironically, like the shock-related peak in October, the peak

on day 72 does not exhibit a softening of the spectrum but rather marks the end of a gradual softening of the spectrum which occurred over the preceding days and the beginning of a hardening of the spectrum over the final days of the event. Commensurate with the overall softer spectra, incident protons from this event did not produce ground level neutron enhancements.

CONCLUSIONS

We have investigated the solar energetic particle flux during 1989 using Los Alamos CPA detectors, concentrating on four 10-day intervals with peak fluxes greater than 10^3 $(cm^2\ s\ sr)^{-1}$. Each of the events within these four intervals shows a unique signature and none conform with the most common expectations for a "typical" SEP event. In all four intervals the effects of the activity of the source region, its motion on the solar surface, magnetic connectivity to the Earth, and propagation within the solar wind are apparent in the flux profiles. Without detailed solar wind monitoring data (which is not available for 1989) a full understanding of all the features in the flux profile is not possible. Nevertheless, we have investigated the broad morphology of each event and have drawn attention to particular source and propagation effects. We have measured the characteristic rise and decay times for these events. Using simulations of the instrument response and assuming the spectrum is of exponential form, we have calculated the spectral slope as a function of time and compared its evolution to the flux levels and also to ground level neutron events. We have also considered how propagation through the disturbed solar wind can change the temporal evolution of fluxes and spectra. In particular, we have pointed out the close association between the passage of an interplanetary shock on day 293 (October 20) and its associated sudden commencement with a sudden, brief, order-of-magnitude increase in the fluxes of >10-MeV protons. The same event shows an abrupt decreases in the flux of trapped energetic (> 30 keV) electrons followed by periodic enhancements of flux due to substorms. This geomagnetic activity is also reflected in very high *Kp* levels. We have compared the October event to the August event which shows comparatively little geomagnetic activity indicative of the dramatically different solar wind conditions produced by the early flares in the two events. While geomagnetic activity is not produced by the energetic solar protons it originates in the same solar activity and, as in the March event, may cause dramatic effects on humans and man-made systems.

Acknowledgments. The authors would like to thank T. A. Fritz, R. C. Reedy, and the two referees for valuable discussions and suggestions. This work was done under the auspices of the U.S. Department of Energy and was supported in part by the Geosciences Program of the DoE Office of Basic Energy Science.

The Editor thanks E. Roelof and D. Venkatesan for their assistance in evaluating this paper

REFERENCES

Baker, D. N., R. D. Belian, P. R. Higbie, and E. W. Hones, Jr., High-energy magnetospheric protons and their dependence on geomagnetic and interplanetary conditions, *J. Geophys. Res.*, *84*, 7138, 1979.

Beeck, J., G. M. Mason, R. G. Marsden, D. C. Hamilton, and T. R. Sanderson, Injection and diffusive transport of suprathermal through energetic solar flare protons (35 keV to 20 MeV), J. *Geophys. Res., 95*, 10,279, 1990.

Belian, R. D., D. N. Baker, P. R. Higbie, and E. W. Hones, Jr., High-resolution energetic particle measurements at 6.6 R_E, 2, High-energy proton drift echoes, *J. Geophys. Res., 83*, 4857, 1978.

Belian, R. D., D. N. Baker, E. W. Hones, and P. R. Higbie, High-energy proton drift echoes: Multiple peak structure, *J. Geophys. Res., 89*, 9101, 1984.

Bieber, J. W., P. Evenson, and M. A. Pomerantz, A barrage of relativistic solar particle events, *Eos Trans. AGU,, 71*, 1027, 1990.

Cane, H. V., D. V. Reams, and T. T. von Rosenvinge, The role of interplanetary shocks in the longitude distribution of solar energetic particles, *J. Geophys. Res., 93,* 9555, 1988.

Freier, P. S., and W. R. Webber, Exponential rigidity spectrums for solar-flare cosmic rays, *J. Geophys. Res., 68*, 1605, 1963.

Gorney, D. J., Solar cycle effects on the near-Earth space environment, *Rev. Geophys., 28*, 315, 1990.

Higbie, P. R., R. D. Belian, and D. N. Baker, High-resolution energetic particle measurements at 6.6 R_E, 1, Electron micropulsations, *J. Geophys. Res., 83*, 4851, 1978.

Kahler, S. W., E. W. Cliver, H. V. Cane, R. E. McGuire, R. G. Stone, and N. R. Sheely, Jr., Solar filament eruptions and energetic particle events, *Astrophys. J., 302*, 504, 1986.

Mathews, T, and D. Venkatesan, Unique series of increases in cosmic-ray intensity due to solar flares, *Nature, 345*, 600, 1990.

McCracken, K. G., and U. R. Rao, Solar cosmic ray phenomena, *Space Sci. Rev., 11*, 155, 1970.

McCracken, K. G., U. R. Rao, R. P. Bukata, and E. P. Keath, The decay phase of solar flare events, *Sol. Phy., 18*, 100, 1970.

McGuire, R. E., and T. T. von Rosenvinge, The energy spectra of solar energetic particles, *Adv. Space Res., 4*, 117, 1984.

Morfill, G., and M. Scholer, Study of the magnetosphere using energetic solar particles, *Space Sci. Rev., 15,* 267, 1973.

Reeves, G. D., T. A. Fritz, T. E. Cayton, and R. D. Belian, Multi-satellite measurements of the substorm injection region, *Geophys. Res. Lett., 17,* 2015 1990.

Reeves, G. D., R. D. Belian and T. A. Fritz, Numerical tracing of energetic particle drifts in a model magnetosphere, *J. Geophys. Res., 96,* 13,997, 1991.

Roelof, E. C., and S. M. Krimigis, Analysis and synthesis of coronal and interplanetary energetic particle, plasma, and magnetic field observations over three solar rotations, *J. Geophys. Res., 78*, 5375, 1973.

Smart, D. F., and M. A. Shea, Galactic cosmic radiation and solar energetic particles, in *Handbook of Geophysics and the Space Environment,* Chap. 6, edited by A. S. Jursa, U.S. Dep. of Comm., Washington, D. C., 1985. (Available as NTIS AD/A167-000 from Natl. Tech. Inf. Serv. Springfield, VA.)

Smart, D. F., and M. A. Shea, Solar proton events during the past three solar cycles, *J. Spacecr. Rockets, 26,* 403, 1989.

Zeigler, J. F., J. P. Biersack, and U. Littmark, *The Stopping and Range of Ions in Solids,* Pergamon Press, new York, 1985.

R. D. Belian, T. E. Cayton, S. P. Gary, and G. D. Reeves, Los Alamos National Laboratory, Los Alamos, NM 87545.

(Received May 20, 1991;
revised November 11, 1991;
accepted December 6, 1991.)

Paper number 91JA03102.
0148-0227/92/91JA-03102$05.00

Fig. 1. One-hour average fluxes of protons with energies greater than 10 MeV observed by spacecraft 1987-097 during 1989. During six intervals, fluxes exceeded 10^3 $(cm^2\ s\ sr)^{-1}$. Numerous events with smaller fluxes are also observed marking 1989 as the one of the most active years in the space era.

Fig. 2. One hour average, >10-MeV proton fluxes over 10-day intervals including six of the most significant SEP events of 1989. The plus symbols indicate the time and intensity of peak fluxes observed by the GOES spacecraft and reported by the Space Environment Lab. Arrows mark the times of *X* class flares observed during these intervals. The black arrows represent the source flare identified in "Solar Geophysical Data Prompt Reports, 1989" and gray arrows represent other flares.

Fig. 3. Expanded views of the onset of the August and October A events. The upper panel in each plot shows the flux of electrons with trapped energies greater than 30 keV and solar protons with energies greater than 10 MeV. The lower panel shows the 3-hour *Kp* indices for these intervals. The upward pointing arrow marks the onset of a sudden commencement event at the Earth.

Fig. 4. A comparison of the measured and model count rates in channels 8 to 16 of the HiP detector. Model count rates were obtained from the convolution of the detector energy response function with an assumed spectrum. The spectrum used is an exponential in rigidity with the spectral slope given by a best fit to the measured count rates.

Fig. 5. Two sample spectra. Flux is plotted as a function of rigidity for day 292, 1800 UT, near the onset of the October A event, and for day 293, 1507 UT at the peak of the shock-related proton flux enhancement. The earlier time shows lower overall fluxes but a much harder spectrum. (The derivation of the spectra is explained in the text.)

Fig. 6. The spectral slope (top panel) and fluxes (bottom panel) for each of the four intervals. Spectral slope γ is determined from a best fit to an exponential in rigidity of the form $F \quad \exp(\gamma R)$. The spectral slopes are fit to one-hour average flux data. Times of ground level neutron enhancements are indicated by upward pointing triangles.

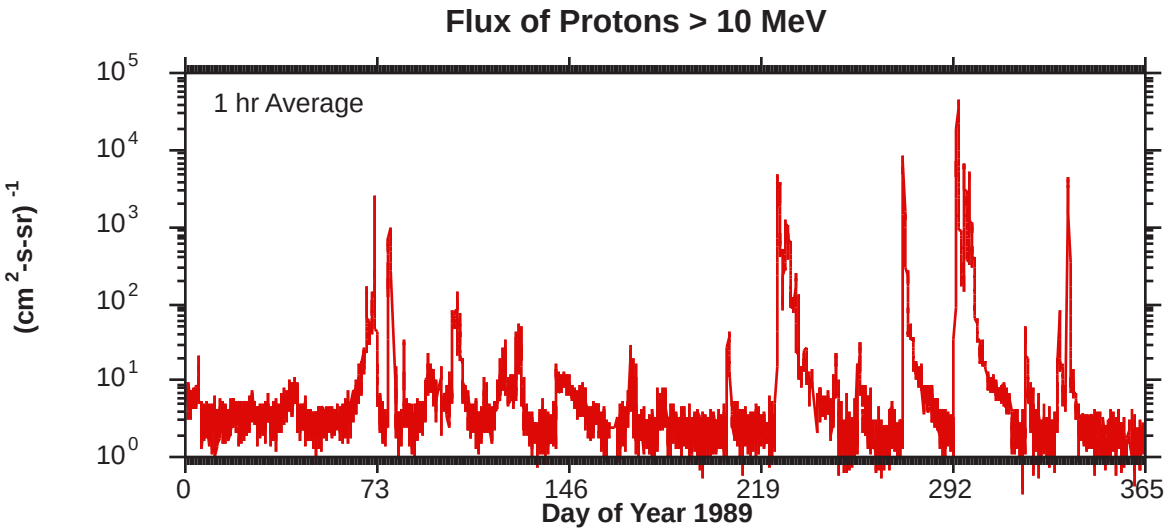
Flux of Protons > 10 MeV
1 hr Average
(cm -2-s-sr) -1
10 5
10 4
10 3
10 2
10 1
10 0
0
73
146
219
292
365
Day of Year 1989

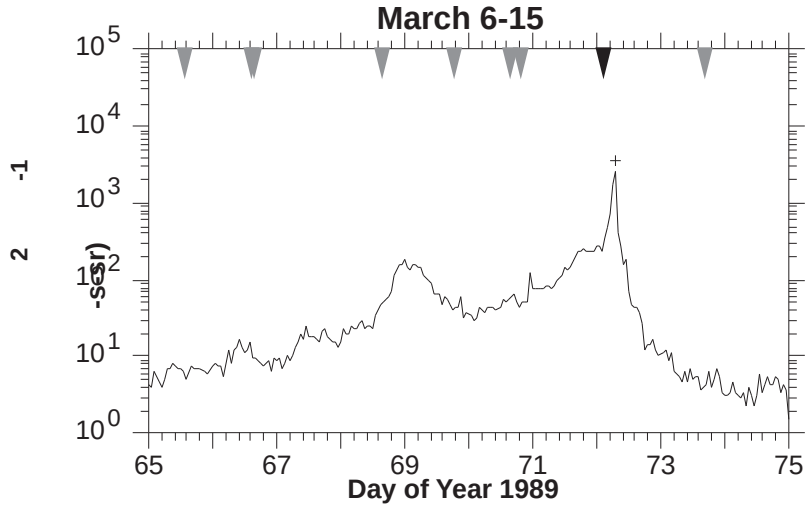
March 6-15
10^5
10^4
10^3
10^2
10^1
10^0
2 -1
-s-sr)
65
67
69
71
73
75
Day of Year 1989

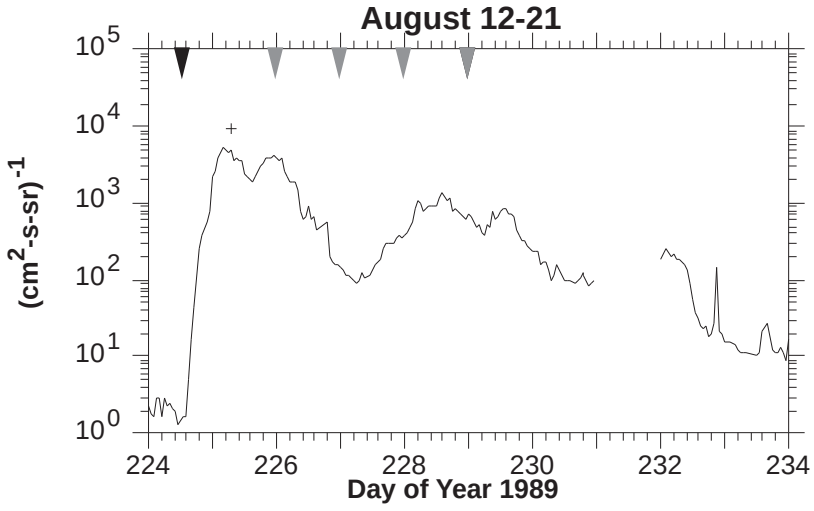
August 12-21
10^5
10^4
10^3
10^2
10^1
10^0
$(cm^2\text{-s-sr})^{-1}$
224
226
228
230
232
234
Day of Year 1989

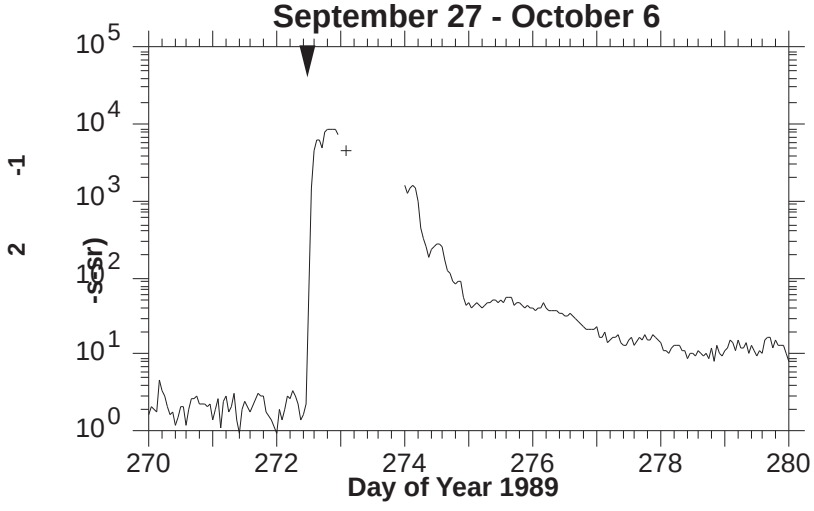
September 27 - October 6
10^5
10^4
10^3
10^2
10^1
10^0
2 -1
-s-sr)
270
272
274
276
278
280
Day of Year 1989

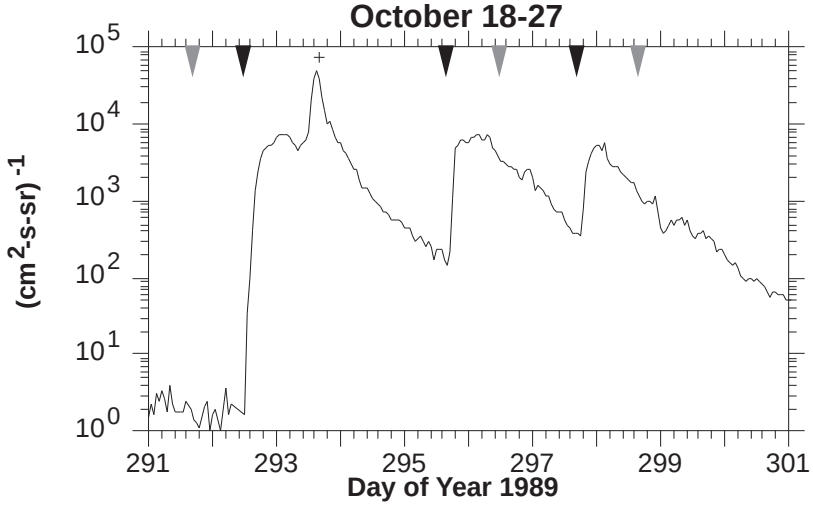
October 18-27
10^5
10^4
10^3
10^2
10^1
10^0
$(cm^2\text{-s-sr})^{-1}$
291
293
295
297
299
301
Day of Year 1989

Figure 3 could not be reproduced electronically

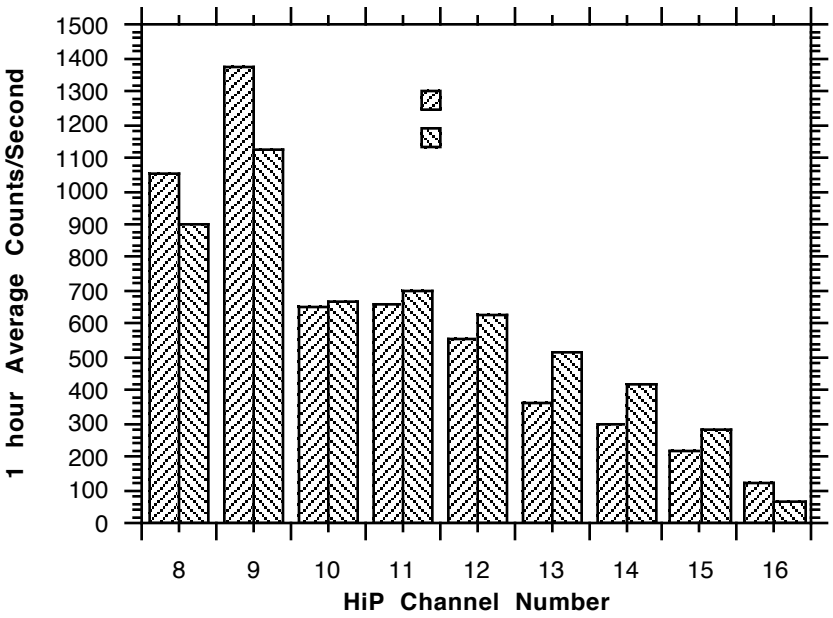
1 hour Average Counts/Second
1500
1400
1300
1200
1100
1000
900
800
700
600
500
400
300
200
100
0
8
9
10
11
12
13
14
15
16
HiP Channel Number

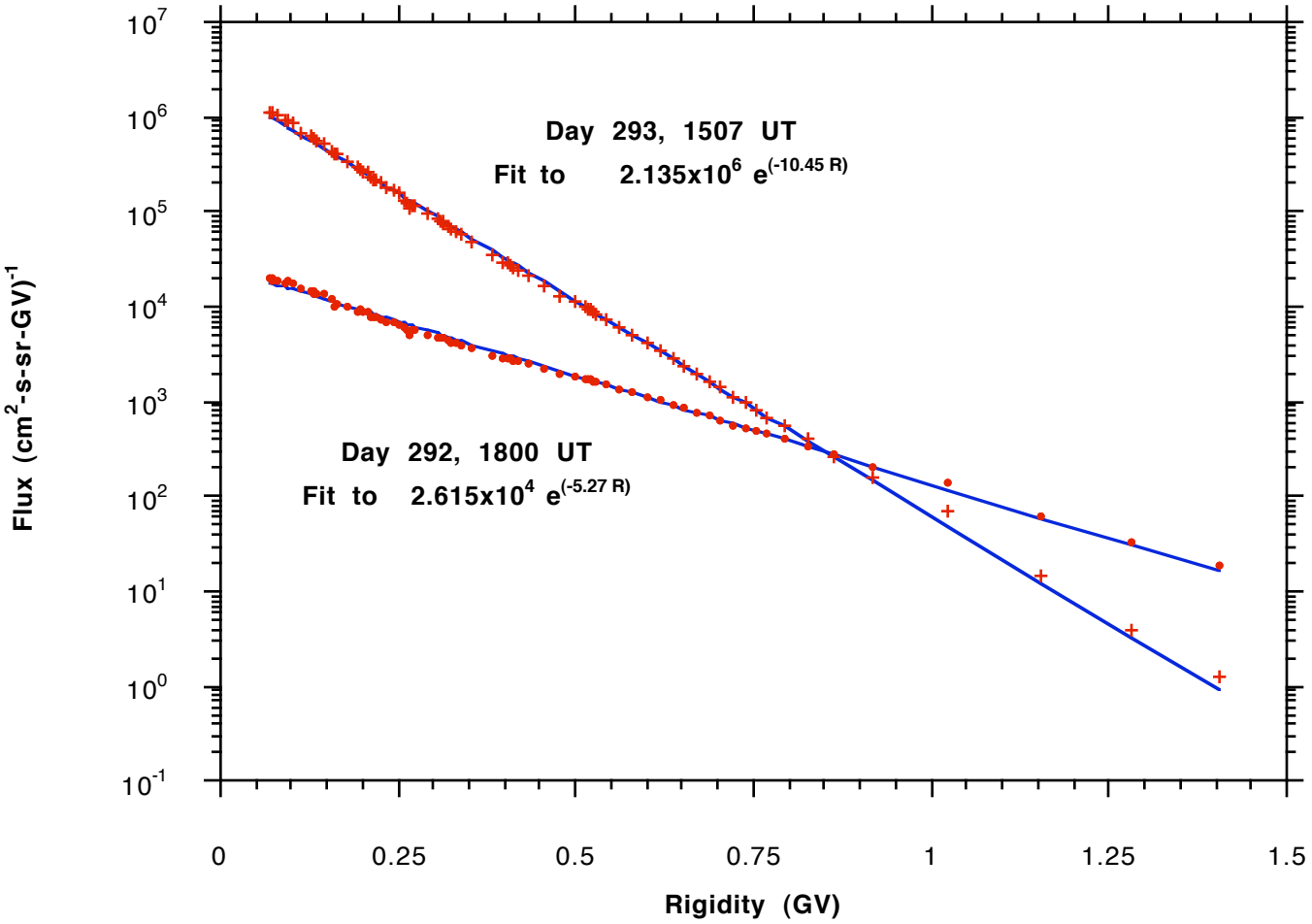
Day 293, 1507 UT
Fit to 2.135x10^6 e^(-10.45 R)
Day 292, 1800 UT
Fit to 2.615x10^4 e^(-5.27 R)
Flux (cm^2-s-sr-GV)^-1
Rigidity (GV)
10^7
10^6
10^5
10^4
10^3
10^2
10^1
10^0
10^-1
0
0.25
0.5
0.75
1
1.25
1.5

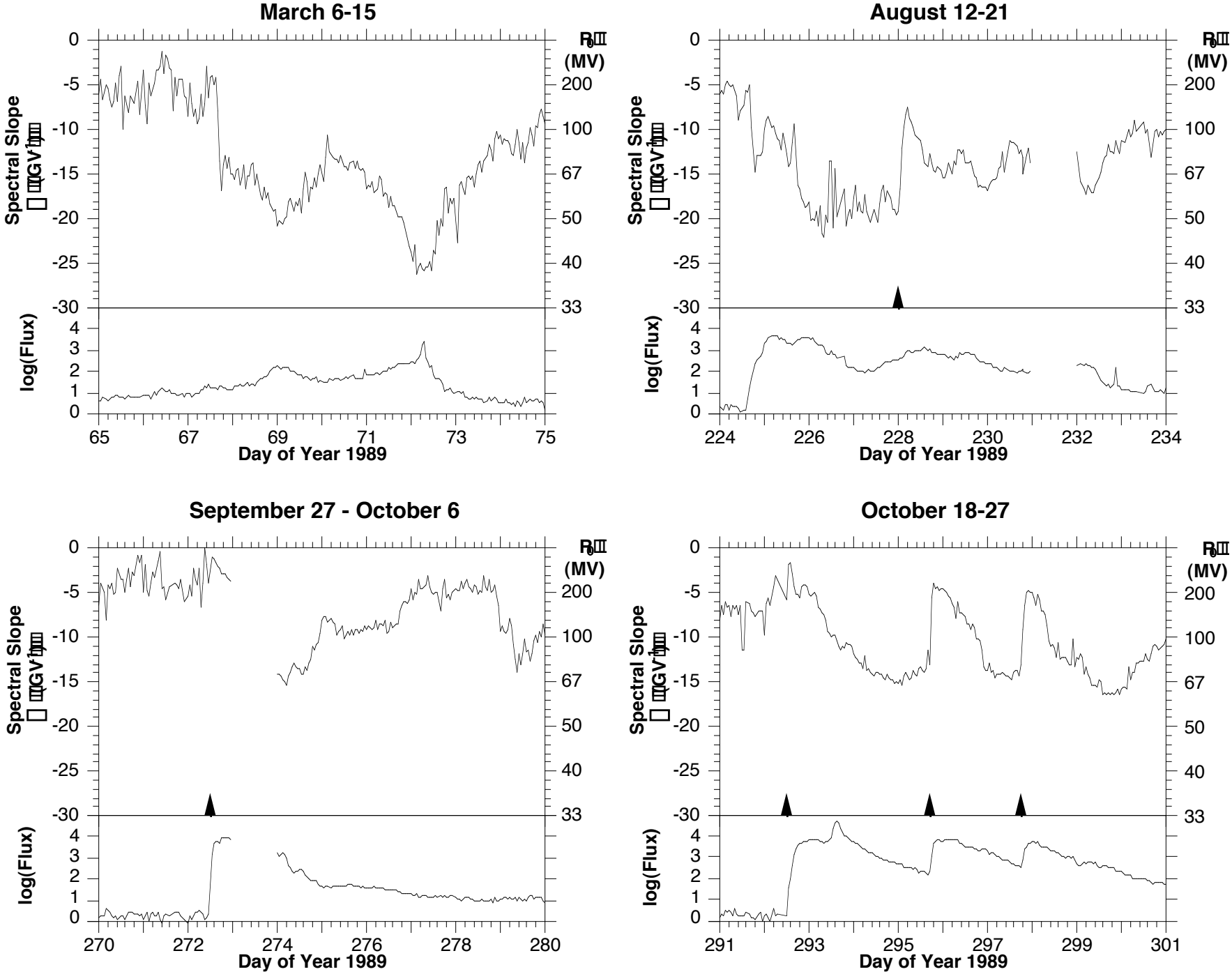
March 6-15
August 12-21
September 27 - October 6
October 18-27
Spectral Slope
log(Flux)
Day of Year 1989
(MV)

TABLE 1. Characteristic Properties for Six Events Identified in the Four Selected Intervals

Event	t_{max} day	t_{max} hour	Max Flux $(cm^2\ s\ sr)^{-1}$	Fluence > 10 MeV $(cm^2\ sr)^{-1}$	τ_{rise}, hours	τ_{decay}, hours	Source Longitude
March	72	07	2542.0	5.93×10^7	1.0	3.6	2° W
August	225	04	4996.0	5.63×10^8	1.2	12.5	37° W
September	272	20	8306.7	6.82×10^8	0.3	9.9	90° W
October A	293	15	45899.0		0.8	7.3	10° E
October B	296	03	6861.6	2.17×10^9	0.3	12.7	31° W
October C	298	03	5403.4		0.8	13.3	55° W

TABLE 2. Times and Intensities of Ground Level Neutron Enhancements

Date	Onset, UT	I_{max}
August 16	0135	12.6
September 29	1150	405.6
October 19	1305	47.4
October 22	1800	30.1
October 24	1825	106.7

Data are from *Mathews and Venkatesan* [1990]. Intensities are given as a percentage increase over preevent levels